atmosphere

MDPI

Article

Analysis of the Diurnal, Weekly, and Seasonal Cycles and Annual Trends in Atmospheric CO_2 and CH_4 at Tower Network in Siberia from 2005 to 2016

Dmitry Belikov [1,*], Mikhail Arshinov [2], Boris Belan [2], Denis Davydov [2], Aleksandr Fofonov [2], Motoki Sasakawa [3] and Toshinobu Machida [3]

1 Center for Environmental Remote Sensing, Chiba University, 1–33 Yayoi-cho, Inage-ku, Chiba 263-8522, Japan
2 V.E. Zuev Institute of Atmospheric Optics, Russian Academy of Sciences, Tomsk 634055, Russia; michael@iao.ru (M.A.); bbd@iao.ru (B.B.); denis@iao.ru (D.D.); alenfo@iao.ru (A.F.)
3 Center for Global Environmental Research, National Institute for Environmental Studies, Tsukuba, Ibaraki 305-8506, Japan; sasakawa.motoki@nies.go.jp (M.S.); tmachida@nies.go.jp (T.M.)
* Correspondence: d.belikov@chiba-u.jp

Received: 27 August 2019; Accepted: 29 October 2019; Published: 8 November 2019

Abstract: We analyzed 12 years (2005–2016) of continuous measurements of atmospheric CO_2 and CH_4 concentrations made at nine tower observation sites in the Japan–Russia Siberian Tall Tower Inland Observation Network (JR-STATION), located in Siberia. Since the data are very noisy and have a low temporal resolution due to gaps in instrument operation, we used the recently developed Prophet model, which was designed to handle the common features of time series (multiple strong seasonalities, trend changes, outliers) and has a robust performance in the presence of missing data and trend shifts. By decomposing each sampled time-series into its major components (i.e., annual trend and seasonal, weekly, and hourly variation), we observed periodically changing patterns of tracer concentrations. Specifically, we detected multi-year variability of tracers and identified high-concentration events. The frequency of such events was found to vary throughout the year, reaching up to 20% of days for some months, while the number of such events was found to be different for CO_2 and CH_4. An analysis of weather conditions showed that, in most cases, high-concentration events were caused by a temperature inversion and low wind speed. Additionally, wind directions were found to be different for high- and low-concentration events. For some sites, the wind direction indicated the location of strong local sources of CO_2 and CH_4. As well as elucidating the seasonality of greenhouse gas concentrations, this study confirmed the potential of the Prophet model for detecting periodicity in environmental phenomena.

Keywords: methane; carbon dioxide; greenhouse gas emissions

1. Introduction

Detailed information on the distribution of sources and sinks of the atmospheric greenhouse gases (GHGs) CO_2 and CH_4 is a prerequisite for analyzing and understanding the role of the carbon cycle within the context of global climate change. Within the context of global climate change, accurate continuous long-term measurements in Siberia are particularly crucial for estimating global CO_2 and CH_4 budgets due to potential changes in natural emissions from the biosphere, wetlands, thawing lakes, and melting permafrost. Siberia is considered to be one of the world's largest carbon reservoirs due to its large forest

area [1,2]. Therefore, it is important to accurately measure CO_2 and CH_4 concentrations in this region. In 2002, the National Institute for Environmental Studies (NIES) began a cooperative project for the continuous measurement of greenhouse gases in West Siberia called the Japan–Russia Siberian Tall Tower Inland Observation Network (JR-STATION). The number of observational sites has been progressively expanded, and the network now consists of nine towers, eight located in West Siberia and one located in Yakutsk, East Siberia [3].

Previous studies have performed detailed analysis of data subsets for individual towers in Siberia [3–8] with the highest density of observations. An analysis of the diurnal behavior of CO_2 and CH_4 concentration in West Siberia was described in Arshinov et al. [5]. A variation of CO_2 due to changes in the height of the planetary boundary layer (PBL) was studied in [7]. For a more complete understanding of concentration variations, it is necessary to perform an analysis over a long period for all JR-STATION sites simultaneously. However, such work required advanced statistical methods to handle noisy time-series with large gaps.

The establishment of JR-STATION improved the observation coverage providing a more accurate estimate of middle- and high-latitude fluxes and their inter-annual variability [9–11]. However, only a limited part of the measurements was used, as very strong data selection criteria were applied to avoid assimilating observations caused by large and not normally distributed values of the model representation errors. For example, in [11] all observations for times when the vertical temperature gradient from the lower to upper level was positive indicating atmospheric inversion conditions, and when the wind speed was below 3 m/s. Thus, a large percentage of the data was excluded. For better use of observations in inversions, it is necessary to develop more optimal criteria for filtering outliers, which requires an understanding of the processes of formation of temperature inversions and their influence on the concentration of tracers.

The commonly used time-series analysis methods (e.g., different types of moving average), usually work well but have a tendency to generate large errors when changes happen in the trends. A new time-series forecasting model Prophet, recently developed by Facebook, adopts a generalized additive model to fit the smoothing and forecasting functions [12]. The model released a open source package (available both for R and Python) providing a fitting procedure, interactive and flexible specifications, a robust forecasting function in the presence of outliers, missing data, and shifts in the trend and the ability to model multiple periods of seasonality simultaneously. In most of the experimental results, Prophet performs better than any other approach as shown by the authors. The Prophet model was previously used and evaluated in various analysis including atmospheric studies and air quality assessment [13,14].

The main objective of this study was to explore the daily, weekly, and yearly variability of CO_2 and CH_4 concentrations as observed at JR-STATION over a period of 12 years (2005–2016) using the Prophet model. The observational data and the Prophet model are described in Section 2, the results of the data analysis and a discussion are provided in Section 3, and conclusions are drawn in Section 4.

2. Method

2.1. Data

This study used datasets which were measured at two different elevations at nine towers in JR-STATION, Siberia Azovo (AZV), Berezorechka (BRZ), Demyanskoe (DEM), Igrim (IGR), Karasevoe (KRS), Noyabrsk (NOY), Savvushka (SVV), Vaganovo (VGN), Yakutsk (YAK) as shown in Table 1. Although the BRZ tower was equipped for sampling at four elevations, only data from the two upper elevations were selected. The observation towers were distributed over a wide area encompassing different biome types. The BRZ tower is located in the middle of taiga (boreal forest); the DEM, KRS, and NOY towers are located in a forest zone and are surrounded by extensive wetlands; and the IGR tower is situated in the small town of Igrim (population of about 10,000), which is located next to the Ob River and is surrounded by extensive wetlands. Additionally, three towers—AZV, VGN, and SVV, are located in a steppe region.

The VGN tower is situated 100 km southeast of the city of Chelyabinsk, while the AZV tower is situated 30 km southwest of the city of Omsk; both cities have a population of over 1 million. The SVV tower is located 1 km south of a small village. The final tower, YAK, is located in East Siberia. The locations of the nine towers are depicted in Figure 1, which also shows natural emissions of CH_4 (mg/m^2/day) derived from CarbonTracker-CH_4 assimilation system v. 2016 [15,16]. Note, JR-STATION tower data are not assimilated by CarbonTracker.

Table 1. Tower sites in the Japan–Russia Siberian Tall Tower Inland Observation Network (JR-STATION), Siberia.

#	Identifying Code	Location	Lat., °	Lon., °	Air Inlet Heights, m	Period of Observations, Years (Data Coverage %)	
						CO_2	CH_4
1	AZV	Azovo	54.71	73.03	29, 50	9 (79)	4 (46)
2	BRZ	Berezorechka	56.15	84.33	40, 80	7 (19)	4 (10)
3	DEM	Demyanskoe	59.79	70.87	45, 63	12 (68)	10 (70)
4	IGR	Igrim	63.19	64.41	24, 47	9 (85)	10 (82)
5	KRS	Karasevoe	58.25	82.42	35, 67	12 (70)	10 (74)
6	NOY	Noyabrsk	63.43	75.78	21, 43	12 (53)	8 (37)
7	SVV	Savvushka	51.33	82.13	27, 52	9 (58)	1 (68)
8	VGN	Vaganovo	54.50	62.32	42, 85	9 (75)	7 (56)
9	YAK	Yakutsk	62.09	129.36	11, 77	8 (58)	6 (28)

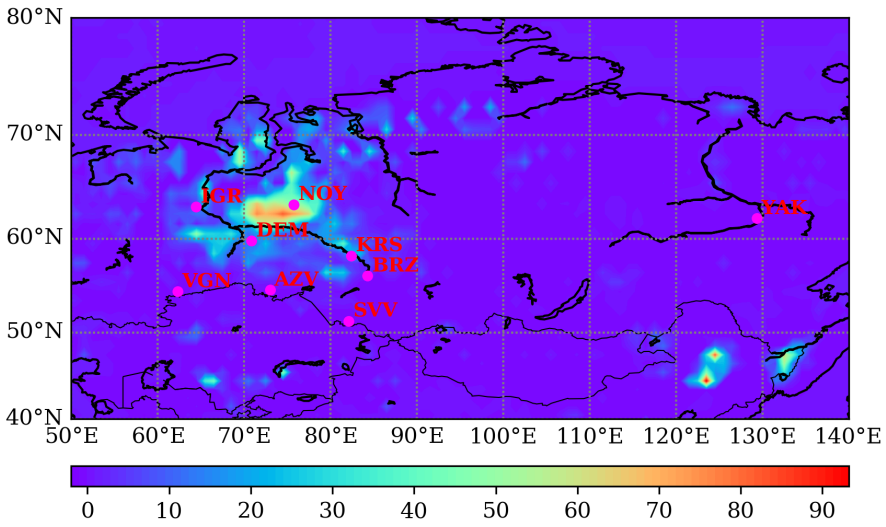

Figure 1. The locations of the measurement towers in the Japan–Russia Siberian Tall Tower Inland Observation Network (JR-STATION), Siberia. Also shown are the natural emissions of CH_4 (mg/m^2/day) estimated by CarbonTracker-CH_4 [15] averaged from 2000 to 2010.

Emissions of CH_4 from wetlands have a significant impact on the greenhouse-gas budget of Siberia. As will be shown below, the location of the measurement station relative to the emission zones is the most important factor for determining the temporal pattern of CH_4 concentrations.

The detailed description of measurement systems applied for the observation sites is published in [3,17]. In the developed CO_2 measurement system the concentration is defined as the mole fraction in dried air using a nondispersive infrared analyzer (model LI-820, LI-COR, USA; a model LI-7000 was used until September 2008 at BRZ). For that purpose, a triple dehumidification system including adiabatic expansion in a glass water trap, a semipermeable membrane dryer (model PD-625–24SS, Permapure, USA), and a magnesium perchlorate trap was employed. With an established standard gas saving system the developed measurement system keeps the analysis precision within 0.3 ppm [17].

For CH_4 measurements, a tin dioxide sensor (TOS) was used. This instrument is precise, cost-effective, low power, low carrier-gas consumption, and high mobility. However, the TOS detects methane and other flammable gases (carbon monoxide, hydrogen, and alcohols) and is sensitive to temperature and water vapor in ambient air. In the developed measurement system the sensitivity to temperature and water vapor was reduced by implementing temperature-stabilization and dehydration of the atmospheric samples by a heater unit and low-pressure water trap with chemical desiccant made of P_2O_5. To avoid the interference of other combustible gases they are removed by an additional catalyst. The overall performance and stability of the TOS sensor for measurements of CH_4 in ambient air were validated using a gas chromatograph equipped with a flame ionization detector (GC/FID). The precision of the system is within 3 ppb [3,18].

In addition to CO_2 and CH_4 concentrations, wind speed and direction (at the high inlet), air temperature and humidity (at all levels), and solar radiation and precipitation (on top of the container laboratory) were measured at the nine JR-STATION towers.

Initially, we planned to analyze hourly averages of atmospheric CO_2 and CH_4 mixing ratios collected at the nine tower sites between 1 January 2005 and 31 December 2016 (12 years); however, such a long dataset was not available for all towers (Table 1). Although the equipment was set up to conduct observations every hour, this was not always technically possible, and the datasets therefore contain many gaps. Hourly measurements of CO_2 and CH_4 cover about 50–80% and 40–70% of the 12 year period, respectively. Significantly fewer measurements are available for the following sites: BRZ (CO_2 and CH_4), AZV (CH_4), SVV (CH_4), and YAK (CH_4) (Table 1). Such extremely low coverage could affect the analysis and distort the results. Therefore, to avoid this, we excluded from consideration the two datasets with the lowest coverage, namely BRZ (CH_4) and SVV (CH_4).

Another issue which could affect the results are the frequent and large fluctuations in concentration due to variations in emissions. The daily mean emissions of CH_4 from Siberian wetlands have been estimated at between 10 and 500 $mg/m^2/day$ [19–22]. The daily variation in CH_4 concentration is much larger than the seasonal variation (e.g., for KRS, see Figure 2e).

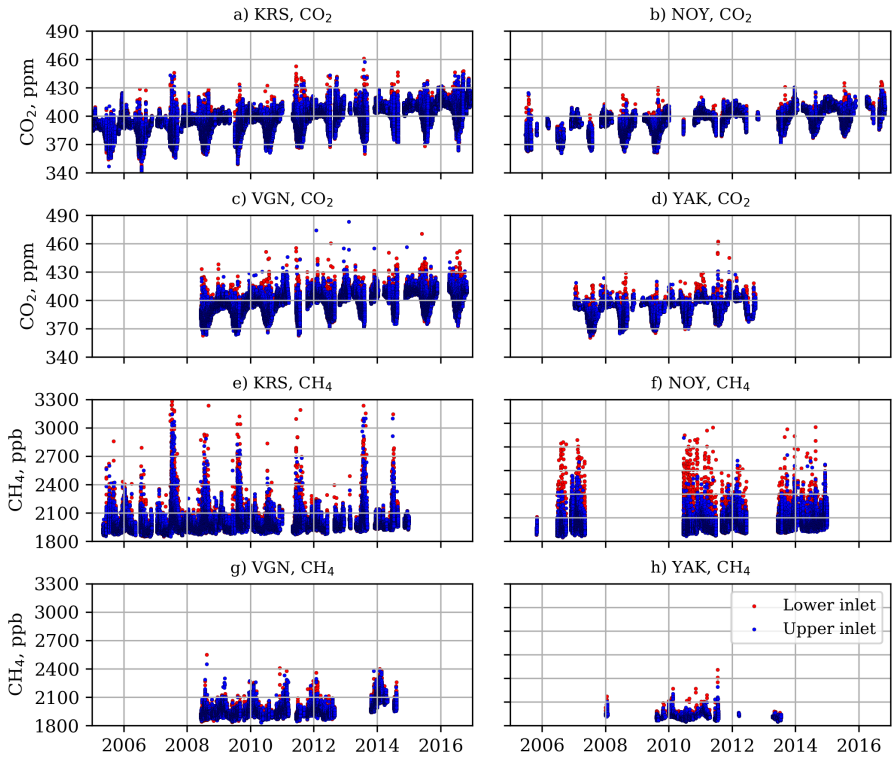

Figure 2. Hourly time-series of CO_2 (**a**–**d**) and CH_4 (**e**–**h**) for the KRS, NOY, VGN, and YAK towers. Red and blue dots represent measurements from the lower and upper inlet, respectively

2.2. The Prophet Model

The Prophet model was designed for the analysis and forecasting of time-series data based on an additive model with three main model components: trend, seasonality, and holidays [23]. These are combined in the following equation [12]:

$$y(t) = g(t) + s(t) + h(t) + e(t) \tag{1}$$

where $g(t)$ is the trend function, $s(t)$ represents periodic changes (e.g., weekly and yearly seasonality), and $h(t)$ represents the effects of holidays which occur on potentially irregular schedules over one or more days. The error term $e(t)$ represents any idiosyncratic changes which are not accommodated by the model. The parametric assumption of [12] shows that $e(t)$ is normally distributed.

Compared to traditional exponential smoothing models, the Prophet model can more easily handle temporal patterns with multiple periods and has no requirements regarding the regularity of measurement spacing. It works best with time-series that have strong seasonal effects and with several seasons of historical data. The Prophet model has a robust performance in the presence of missing data and trend shifts and typically handles outliers well [12]. The large number of gaps that exist in the JR-STATION measurements make the Prophet model particularly suitable to simultaneously reveal the daily, weekly, and monthly seasonality from the hourly time-series.

Prophet includes two trend models $g(t)$ that cover many applications: a saturating growth model, and a piecewise linear model. The logistic growth model in its most basic form is:

$$g(t) = \frac{C}{1 + exp(-k(t - m))}, \tag{2}$$

where C is the carrying capacity, k the growth rate, and m is an offset parameter.

There are two important aspects of growth that can not be captured in Equation (2). First, the carrying capacity is not constant. Thus the fixed capacity C is replaced with a time-varying capacity $C(t)$. Second, the growth rate is not constant. The model must be able to incorporate a varying rate in order to fit historical data. The piecewise logistic growth model is used to overcome those issues:

$$g(t) = \frac{C(t)}{1 + exp(-(k + a(t)^T\delta)(t - (m + a(t)^T\gamma)))}, \quad (3)$$

where the rate at any time t is the base rate k, plus all of the adjustments up to that point: $k + a(t)^T\delta$. The correct adjustment at changepoint is easily computed as $a(t)^T\gamma$ [12].

To provide flexibility for periodic effects, the Prophet model uses the Fourier series [24]:

$$s(t) = \sum_{n=1}^{N} \left(b_n \cos\left(\frac{2\pi nt}{P}\right) + b_n \sin\left(\frac{2\pi nt}{P}\right) \right) \quad (4)$$

where t denotes the time and P represents the regular period that the time-series is expected to have (seven and 365.25 days for the weekly and yearly periods, respectively). Fitting seasonality requires the estimation of the $2N$ parameters $\beta = [a_1, b_1, ..., a_N, b_N]^T$. This was done by constructing a matrix of seasonality vectors for each value of t in the historical data.

3. Results and Discussion

The Prophet model was implemented to analyze the time-series measured at towers in the JR-STATION, Siberia (Table 1).The trend and seasonal variation of the time-series analyzed in the present study have been analyzed for individual sites in past publications. Therefore, here we restricted the analysis to comparing CO_2 and CH_4 data between sites while paying more attention to short-term changes [3–8]. To analyze annual trends, and seasonal and weekly variation we use daytime (11:00–18:00 local time) observations only, while for daily variation all measurements were used.

The Prophet model is implemented through the Python package [25]. The flexibility of the trend is controlled by adjusting the number of changepoints automatically selected. The periods are set to 365.25 and 7 days. The model's default values for N (i.e., $N = 10$ and $N = 3$ for modeling yearly and weekly components, respectively) were tested first. Though these values have been empirically demonstrated to work well for most practical situations [12], in this work $N = 10$ produces inexplicably large variability in seasonal cycles, so empirically we reduced N to 5.

3.1. Trend

The calculated CO_2 trends (Figure 3a) show a stable growth of about 2 ppm/yr, which corresponds to the global value [26]. The small differences in the CO_2 growth rate that are observed between sites are due to the different lengths of the datasets, the different heights of the sampling inlets, and the influence of local sources. For methane concentrations, the length of the dataset and the number of gaps are important. Therefore, the relatively short SVV dataset was excluded from the analysis, while the AZV, BRZ, and VGN datasets were interpreted with great care.

The observation towers can be grouped based on the average value of the CH_4 concentration (Figure 3b) measured at each one. The highest values of CH_4 concentration were measured at two towers located in the central part of the Vasyugan Swamp (IGR and NOY); medium values were measured at towers located on the outskirts of the Vasyugan Swamp (DEM, KRS); and low values were found at the towers located in West Siberia and furthest from the Vasyugan Swamp (AZV, BRZ, and VGN). The smallest value of CH_4 concentration was measured at YAK, in East Siberia. Measurements from

ground-based networks show that, between 1999 and 2006, atmospheric CH_4 concentrations were nearly constant [27]. From 2007 to 2013, the globally averaged mole fraction of CH_4 in the atmosphere increased by 5.7 ± 1.2 ppb/yr [28]. Most of the CH_4 time-series measured at the JR-STATION towers follow this tendency; however, VGN showed a faster increase after 2012 (as captured by observations Figure 2g), and YAK showed a slower increase for all years.

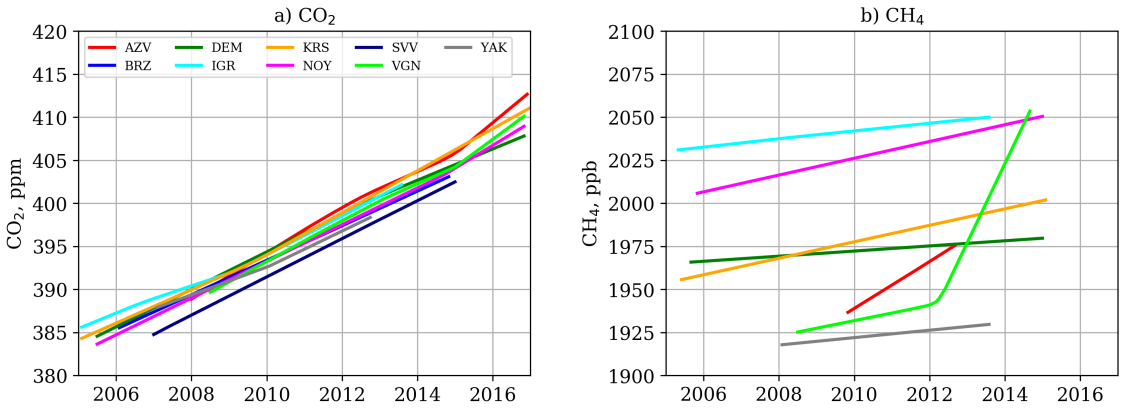

Figure 3. Trends of concentrations of (**a**) CO_2 and (**b**) CH_4 for the JR-STATION tower sites used in this study for the period 2005–2015.

3.2. Seasonal Variation

Measured concentration time-series often have multi-period seasonality as a result of natural and human activity. For instance, the biosphere produces effects that repeat every year, while industrial activities related to a five-day working week can produce effects that repeat every week. Periodic seasonality algorithms should be used to fit such effects. As stated in [12], unlike other statistical models, with the Prophet model, measurements do not need to be regularly spaced in time, and missing values do not need to be interpolated. To derive periodic signals the model uses all the observations for the study period (12 years), thereby increasing accuracy and reducing sensitivity to random outliers, for example generated by forest fires [29]. For some sites, such a strategy is the only one possible to identify the seasonal cycle if the data for different seasons refer to different years. Thus, the derived seasonal variation is generalized and different from that obtained in previous works (i.e., [5,7]).

In the Northern Hemisphere, CO_2 has been shown to exhibit a prominent seasonal cycle with a minimum in July–August and a maximum in November–December, reflecting the metabolic cycles of the land biota. In the present study, the seasonal difference in CO_2 concentration was found to reach up to 30 ppm, which is consistent with previous estimations [4,5,7].

Unlike CO_2, CH_4 concentrations in the Northern Hemisphere are characterized by peaks not only in winter (predominantly due to anthropogenic sources [30]) but also in late summer, caused by emissions from wetlands [5,31]. The CH_4 maximum that was observed in July–August in the present study is consistent with the majority of land surface models used in the inter-comparison study of [21].

The two stations that are furthest from the wetland region (VGN, YAK) showed the lowest summer concentrations of CH_4. A summer peak in CH_4 concentration was measured at KRS, which is located at the border of the lowlands on the downwind side. The amplitude and phase of the CH_4 concentrations measured at DEM, IGR, and KRS are in good accordance with the results of [3].

3.2.1. Case Study: Winter Vacation

For most of the measurement sites, a marked decrease in CO_2 and CH_4 concentrations was observed in late December and the beginning of January (Figure 4a,b). In winter, anthropogenic emissions are the predominant factor behind CO_2 and CH_4 emissions. Therefore, we propose that the decline in concentration in winter is due to reduced industrial and transport activity caused by winter holidays (which usually last about one week [32]).

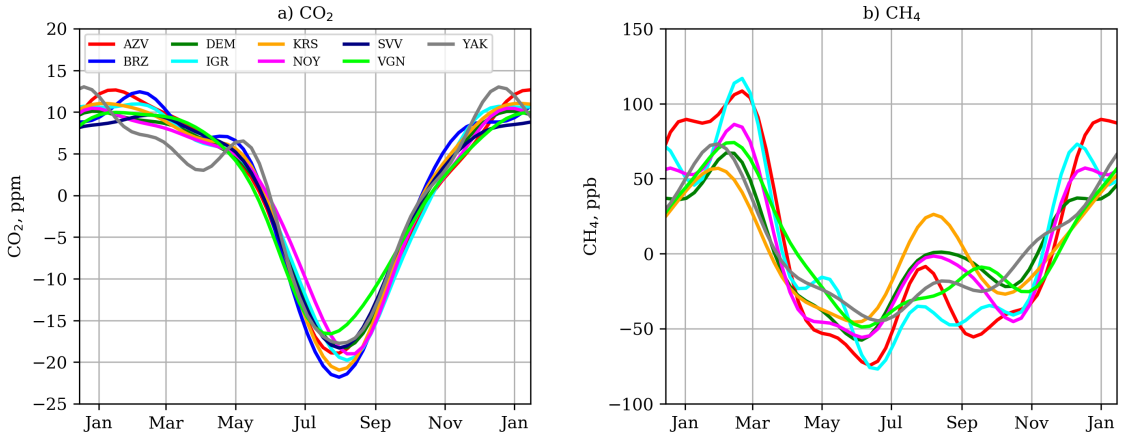

Figure 4. Multi-year (2005–2015) seasonal variation of concentrations of (**a**) CO_2 and (**b**) CH_4 for the considered sites.

To test this hypothesis, we analyzed the concentrations of tracers in the first 10 day period (1–10 January) and second 10 day period (11–20 January) of January for all available years. We assumed that the first period, which we termed "Holiday", was associated with low human (industrial and transport) activity, while the second period, which we termed "Working", was associated with normal human activity. However, this division is rather arbitrary, since the length of the holidays varies from year to year. Moreover, some production cycles of enterprises do not always strictly follow the official working calendar. Some industrial processes include preliminary stages with a low load, and therefore produce lower emissions. Additionally, the schedules for holidays and working days may shift during this period.

After removing the trends, the average values of CO_2 and CH_4 concentration were calculated for the "Holiday" and "Working" periods, respectively (Table 2). Student's *t*-test was used to estimate the statistical significance of the difference between "Holiday" and "Working" datasets. For only a few cases did the test indicate a non-significant difference: NOY and SVV for CO_2, AZV, IGR, and YAK for CH_4. The results suggest that, relative to CH_4, the CO_2 concentration is less sensitive to changes in industrial activity; the difference in CO_2 concentration between the two periods does not exceed 1%, while for two stations the difference is negative. This could be due to the intensive heating of private countryside houses or outdoor activities near to the measurement sites.

Table 2. The average difference in CO_2 and CH_4 concentrations observed at the JR-STATION tower sites between the "Holiday" period (1–10 January) and the "Working" period (11–20 January), "Diff." is difference between the "Holiday" and "Working". For BRZ and SVV, CH_4 time-series were not long enough for analysis. Bold font was used to mark statistically insignificant (estimated using Student's *t*-test) values of difference.

#	Identifying Code	Mean CO_2, ppm			Mean CH_4, ppb		
		Working	Holiday	Diff. (%)	Working	Holiday	Diff. (%)
1	AZV	10.52	8.86	1.67 (15.85)	113.84	120.09	**−6.25 (−5.49)**
2	BRZ	13.71	5.89	7.81 (57.00)	-	-	- (-)
3	DEM	8.41	6.83	1.59 (18.87)	60.76	10.76	50.00 (82.29)
4	IGR	9.07	7.54	1.53 (16.91)	31.91	21.45	**10.47 (32.80)**
5	KRS	8.84	6.35	2.49 (28.14)	42.90	6.60	36.29 (84.62)
6	NOY	8.78	9.05	**−0.28 (−3.15)**	67.43	20.46	46.98 (69.66)
7	SVV	6.87	7.27	**−0.39 (−5.76)**	-	-	- (-)
8	VGN	7.52	8.16	−0.65 (−8.58)	54.63	41.24	13.39 (24.51)
9	YAK	8.17	6.71	1.46 (17.91)	52.49	46.93	**5.56 (10.59)**

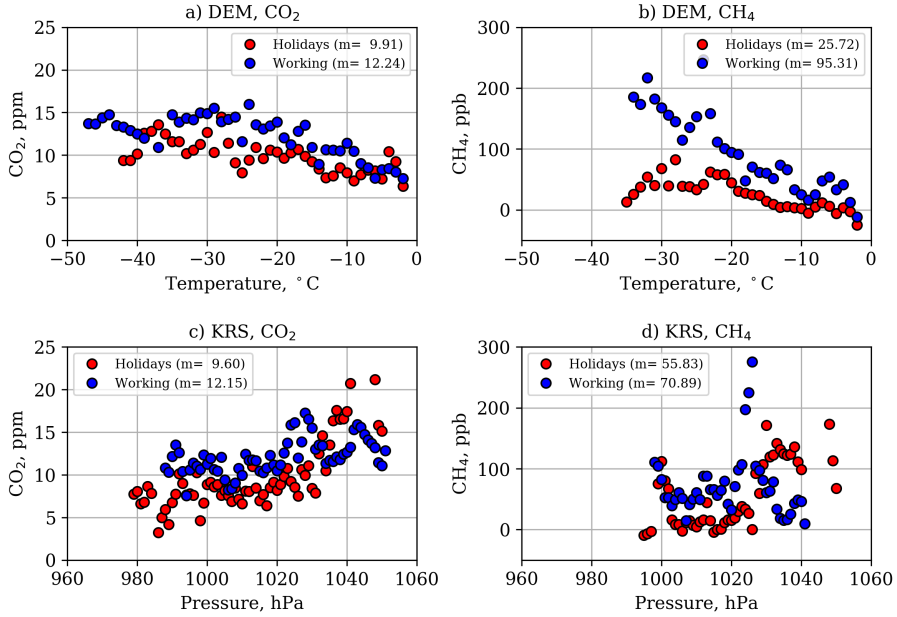

Figure 5. Concentrations of CO_2 and CH_4 versus air temperature (**a**,**b**) and atmospheric pressure (**c**,**d**) for measurement stations DEM and KRS.

Strong high-pressure systems with low air temperature have been observed over Siberia in winter [3], which could potentially affect the measured greenhouse gas concentrations. To exclude the influence of such systems, the distribution of tracers with respect to air temperature (Figure 5a,b) and atmospheric pressure (Figure 5c,d) was considered. The 12 year datasets used for the present study were sufficiently large to analyze greenhouse gas concentrations over a wide range of temperature and pressure. For some sites with decreasing temperature (e.g., DEM), the difference in CO_2 concentration between the "Holiday" and "Working" periods was markedly higher, as more fuel is consumed for heating and transport in the surrounding areas. Therefore, strong high-pressure systems with low air temperature can enhance the effect, but are not the main factors.

3.3. Weekly Variation

The analysis of weekly patterns is useful to identify the tracer emissions associated with industry or transport operating on a five-day working week. Our analysis did not reveal any noticeable features in the distribution of CO_2 concentrations at a weekly scale (Figure 6a). For all sites, the amplitude of the change in CO_2 concentration was less than 1.5 ppm.

For CH_4, the amplitude of the observed change in concentration was larger. However, no clear weekly variation was observed (Figure 6b). This suggests that there were no large anthropogenic sources of CH_4 that constantly affected the concentrations measured at the stations at intervals corresponding to the five-day working week.

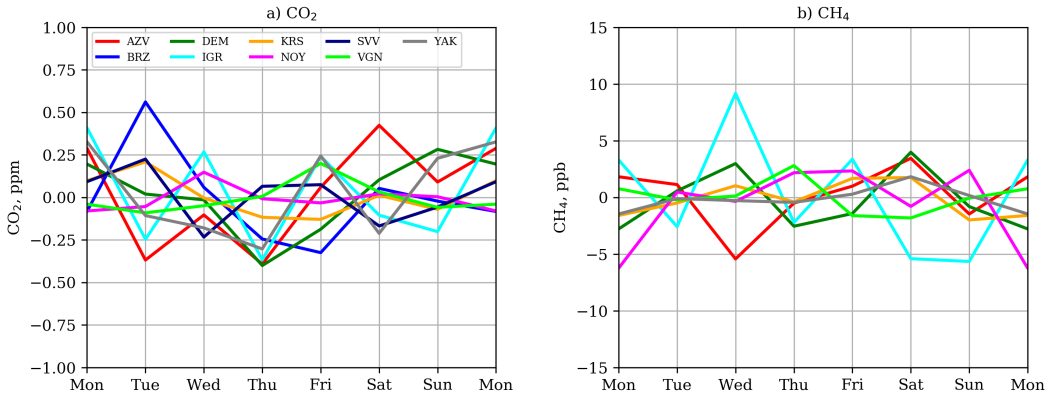

Figure 6. Multi-year (2005–2015) weekly variations of concentrations of (**a**) CO_2 and (**b**) CH_4 derived using the Prophet model for the considered measurement sites.

3.4. Daily Variation

The considered measurement sites are located in the interior of the Asian continent. At such locations, a strong daily change in the height of the planetary boundary layer (PBL) is common. The daily cycle of tracers is most pronounced in summer during dry anticyclonic weather conditions. In this case, frequent surface temperature inversions develop at night and last until the early morning, which impedes vertical atmospheric mixing and traps surface gas emissions in the stable shallow PBL [33]. Concentrations reach maxima in the early morning between 03:00 and 06:00 local time. Minimum concentrations of trace gases emitted from the soil are normally observed between 12:00 and 18:00, when solar heating of the ground induces vertical air turbulence; such turbulence leads to mixing in a deep layer of the atmosphere (approximately 200–600 m deep in winter and up to 2800 m deep in summer [4]).

The magnitude of the nocturnal increase in greenhouse-gas concentrations is variable and depends on the strength of the atmospheric inversion and on the intensity of the regional tracer source. Overcast conditions appear to slow the morning breakup of this inversion so that tracers do not move from the surface layer to high altitudes until 07:00–09:00 [34]. Since precipitation data are also available for the measurement stations used in the present study, it would be interesting to analyze this effect, however, it was not considered in this work.

As shown in Figure 7, concentrations of CO_2 and CH_4 clearly changed throughout the day at all measurement sites. For example, the time-series for NOY is characterized by an evening peak of CH_4 concentration (Figure 7b).

The minimum amplitude of CO_2 and CH_4 daily concentration change (maximum minus minimum concentration) are observed in winter (December–February) while the maximum amplitudes are observed

in summer (June–August), as shown in Table 3. Autumn amplitude values (September–November) are larger than the spring ones (March–May). The mean diurnal variation in CH_4 concentration for each month at the KRS site is shown in [3].

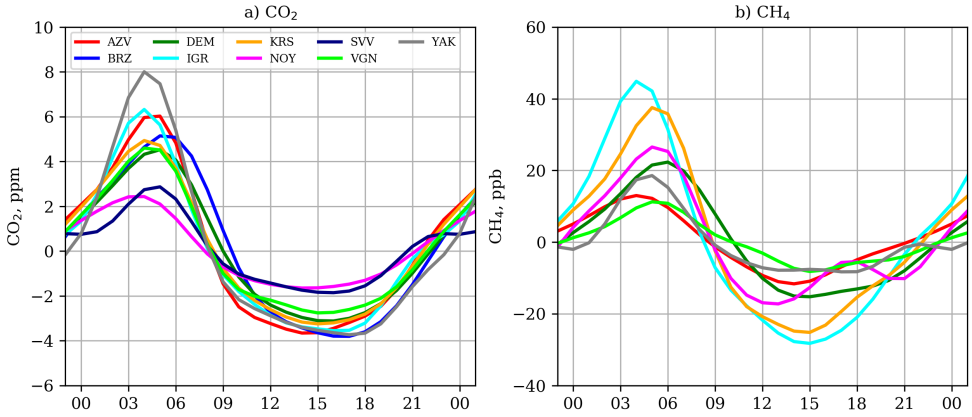

Figure 7. Multi-year (2005–2015) daily variation of the concentrations of (**a**) CO_2 and (**b**) CH_4 derived by the Prophet model for the considered measurement stations.

Table 3. Multi-year (2005–2015) amplitudes of the daily variation of CO_2 and CH_4 concentrations for different seasons for JR-STATION sites in Siberia derived by the Prophet model. Methane data for Yakutsk were not sufficient to assess variations for December-February (DJF), March–May (MAM), June–August (JJA), and September–November (SON).

#	Identifying Code	Amplitude for CO_2, ppm				Amplitude for CH_4, ppb			
		DJF	MAM	JJA	SON	DJF	MAM	JJA	SON
1	AZV	1.04	5.46	26.12	5.20	30.94	21.19	50.68	14.38
2	BRZ	1.24	4.76	23.37	4.54	-	-	-	-
3	DEM	0.61	3.31	20.45	6.63	10.73	22.53	109.42	33.89
4	IGR	1.01	3.66	17.90	9.74	31.27	36.46	146.79	54.20
5	KRS	0.55	3.29	22.07	7.09	11.11	20.06	182.98	41.89
6	NOY	0.24	1.48	10.53	3.48	31.12	37.47	92.62	39.76
7	SVV	0.95	4.12	11.89	3.48	-	-	-	-
8	VGN	0.29	5.45	17.56	3.87	6.39	17.68	52.76	16.75
9	YAK	6.73	6.25	12.46	17.92	-	-	35.04	-

3.5. Diagnostic

Prophet includes functionality of time series nested cross-validation to measure the fitting error using historical data. This is done by selecting cutoff points in the history, and for each of them, fitting the model using data only up to that cutoff point. We can then compare the fitted values to the actual values. This method, called the simulated historical forecasts (SHFs), is based on classical "rolling origin" forecast evaluation procedures [35]. We specify the forecast horizon (365 days), the size of the initial training period (730 days) and the spacing between cutoff dates—period (180 days). Due to the limited number of observations the initial training period for CH_4 for AZV and YAK was reduced to 365 days. Table 4 shows the mean statistics of the fitting performance. The statistics computed are root mean squared error (RMSE), mean absolute error (MAE), and mean absolute percent error (MAPE).

The average error of the model for CO_2 is fairly uniform and does not exceed one percent. For CH_4, the error strongly depends on the location relative to the emission regions (swamps), the length of the time series and the number of observations. Values are in the range of 2–5% (Figure 8). By default Prophet will

only return uncertainty in the trend and observation noise. To get uncertainty in seasonality, it needs to do full Bayesian sampling. We tried different options of the model tuning, but could not determine a method to convert data-density into a calculation of the uncertainty.

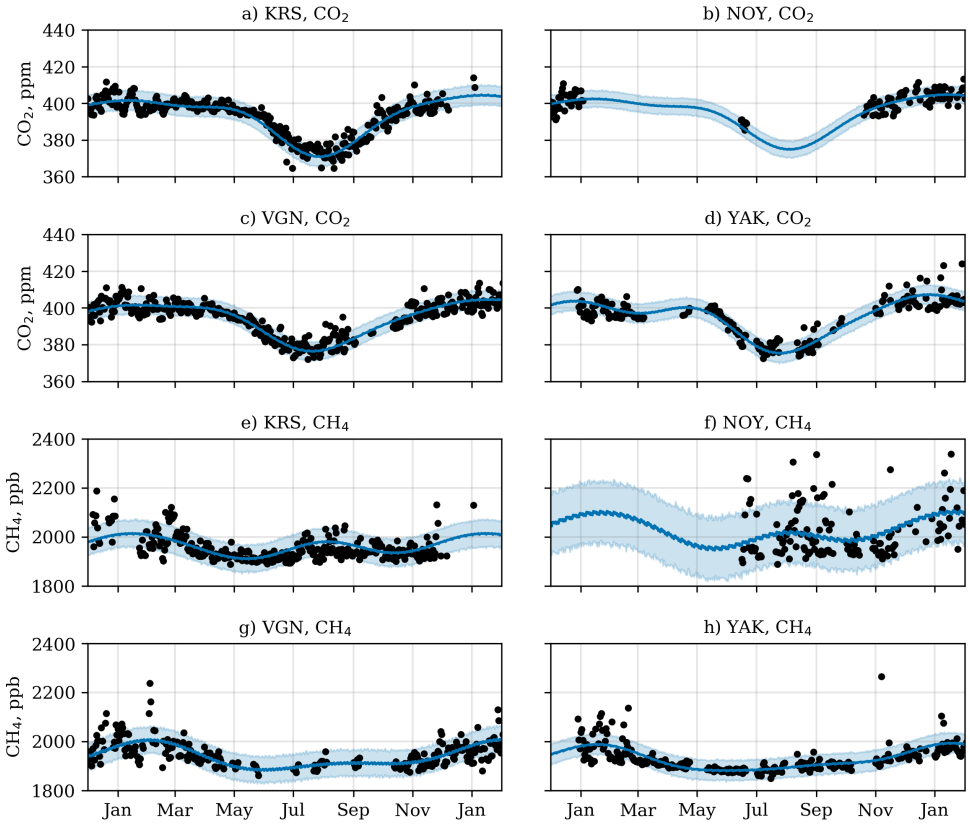

Figure 8. Time-series of CO_2 (**a**–**d**) and CH_4 (**e**–**h**) for the KRS, NOY, VGN, and YAK towers for 2011. Black symbols represent daytime averaged measurements, the blue line is the Prophet model fitting, and the shaded area shows the 80% confidence interval.

Table 4. The Prophet model cross-validation performance metrics at tower network sites in Siberia (JR-STATION). For BRZ and SVV CH_4 data series are not sufficient for analysis. Root mean squared error (RMSE), mean absolute error (MAE), and mean absolute percent error (MAPE).

#	Identifying Code	CO_2			CH_4		
		RMSE	MAE	MAPE (%)	RMSE	MAE	MAPE (%)
1	AZV	4.97	3.84	0.96	48.67	39.96	2.03
2	BRZ	4.43	3.36	0.85	-	-	-
3	DEM	3.97	3.00	0.76	108.77	65.83	3.32
4	IGR	4.92	3.63	0.92	120.91	93.78	4.57
5	KRS	4.36	3.33	0.84	47.64	35.35	1.79
6	NOY	3.76	2.85	0.72	98.66	74.19	3.64
7	SVV	3.91	2.98	0.76	-	-	-
8	VGN	4.25	3.34	0.84	57.10	42.32	2.10
9	YAK	4.76	3.63	0.91	97.49	73.06	3.79

3.6. Temperature Inversion

In order to analyze the effect of temperature inversions in more detail, we examined the difference in the concentrations of CO_2 and CH_4 measured from the lower and upper inlets of the measurement towers for cases with and without inversions (Figure 9). The results show that, for all sites except YAK, inversions have a strong effect on CO_2 concentrations in summer and a relatively weak effect in other seasons (Figure 9d). In the YAK area, temperature inversions consistently form in winter due to the extremely cold and dense air of the Siberian High pooling in deep hollows. In this area, the average minimum temperatures for January, February, and December occasionally fall below −50 °C.

The influence of inversions on CH_4 concentrations is more diverse: For some sites (e.g., KRS; Figure 9e), inversions have as prominent an effect as they do for CO_2 concentrations, while for others (VGN and YAK; Figure 9g,h), concentrations are more uniform throughout the year. However, for two stations located in the very center of the Vasyugan Swamp (IGR and NOY), we did not observe large differences in CO_2 or CH_4 concentrations during temperature inversion (Figure 9f). CH_4 emission is strong throughout the year around NOY.

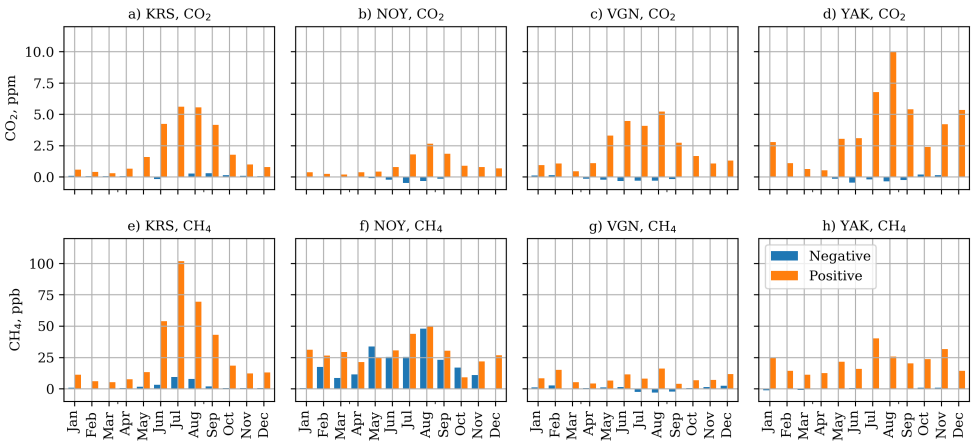

Figure 9. Monthly mean CO_2 (**a**–**d**) and CH_4 (**e**–**h**) concentration difference between lower and upper inlets for events with (Positive) and without (Negative) temperature inversion for KRS, NOY, VGN, and YAK sites, respectively.

Carbon monoxide (CO) emissions usually result from inefficient combustion, and have often been used as a tracer for CO_2 [36]. The ratios of the emissions of CO_2 to CO are different for various combustion and biological processes. Therefore, the simultaneous observation of CO_2 and CO may help to distinguish between fossil fuel sources and terrestrial ecosystem sources of CO_2 [37].

3.7. Elevated Concentration Events

For many types of study (e.g., inverse modeling [9,11,38]), it is important to understand the reason for elevated greenhouse gas concentrations and filter out concentrations caused by local sources or temperature inversions. For a high concentration, we consider the events when the threshold value of concentration is exceeded for three hours or more. The threshold values are selected to be equal to the magnitude of the uncertainty in the concentration calculated by the Prophet model. The threshold values for the considered measurement sites are given in Table 5.

During the study period, the frequency of high-concentration events was 15–20%. The seasonal distribution of these events was not uniform, and is likely to correspond to seasonal variations in

emissions. For CO_2 concentrations, peaks are observed in summer, while for CH_4, summer and winter peaks are observed (Figure 10). For late spring and late autumn, the frequency of events is low. For high-concentration events, the difference in temperature between the upper and lower inlets was analyzed. Since the locations of the inlets are different for different towers, we considered the scaled temperature difference, ΔT_{scaled}, scaled by the height between inlets, ΔH, using the formula:

$$\Delta T_{scaled} = \frac{\Delta T}{\Delta H} * 10. \quad (5)$$

For the IGR, NOY, and VGN towers, in most cases, elevated concentrations are accompanied by a temperature inversion of 0.1–0.3 °C/m. This is also sometimes observed at the KRS tower. At the YAK tower, temperature inversions reached a maximum of 0.5 °C/m during December–January. The strongest summer inversion was observed at the DEM tower.

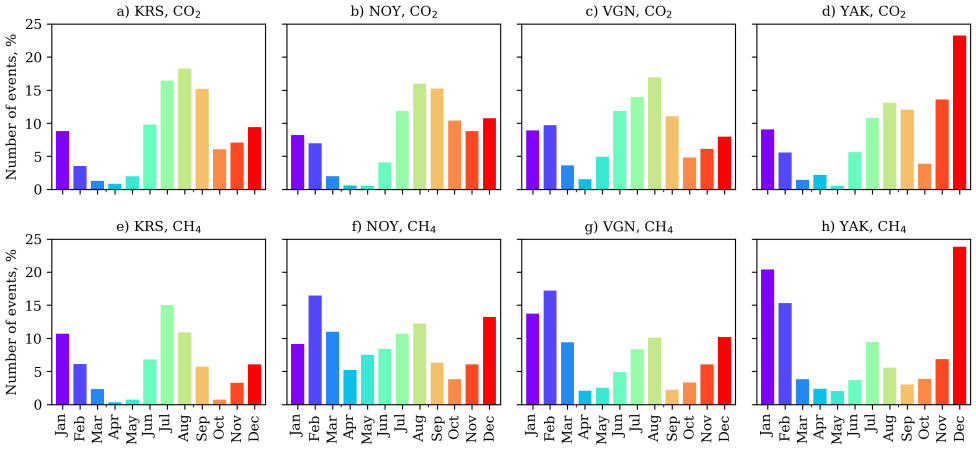

Figure 10. Number of days (%) with elevated concentrations of CO_2 (**a**–**d**) and CH_4 (**e**–**h**) for the KRS, NOY, VGN, and YAK measurement sites.

Table 5. The threshold concentration values for high-concentration events for the considered measurement sites.

#	Identifying Code	Threshold	
		CO_2, ppm	CH_4, ppb
1	AZV	9.33	45.00
2	BRZ	7.81	-
3	DEM	7.47	88.78
4	IGR	8.45	160.51
5	KRS	7.87	98.08
6	NOY	5.57	141.93
7	SVV	5.98	-
8	VGN	7.04	53.49
9	YAK	6.32	39.05

In addition to temperature inversions, low wind speeds have been shown to significantly affect the concentration of tracers in Siberia [39]. Additionally, wind direction also greatly affects the concentration of tracers in Siberia if local sources are located near to the observation site. To identify the effect of wind speed and direction on concentrations of CO_2 and CH_4, we also analyzed events with low tracer concentrations (i.e., concentrations less than the threshold value). A comparison of wind roses for high- and low-concentration events is presented in Figure 11.

From the figure, it is clear that the proposed approach allows wind speeds and directions to be determined for situations with high and low concentrations of CO_2 and CH_4. Since the towers' measurement inlets are located fairly high above the ground, the frequency of calm conditions was very low.

Low wind speeds clearly contribute to the increase of tracer concentrations. However, on the contrary, high wind speeds lead to the faster mixing of air volumes and thus lower tracer concentrations. Importantly, we successfully identified the wind direction which brought more tracer-contaminated air. For the YAK and NOY towers, this corresponded to a fairly narrow range of wind directions (Figure 11). It is very likely that the concentrations at the NOY tower were influenced by CO_2 and CH_4 emissions from the oil and natural gas pipelines which are located several km northwest of the tower [3]. Similarly, the concentrations at the VGN tower were likely influenced by Chelyabinsk, one of the major industrial centers of Russia.

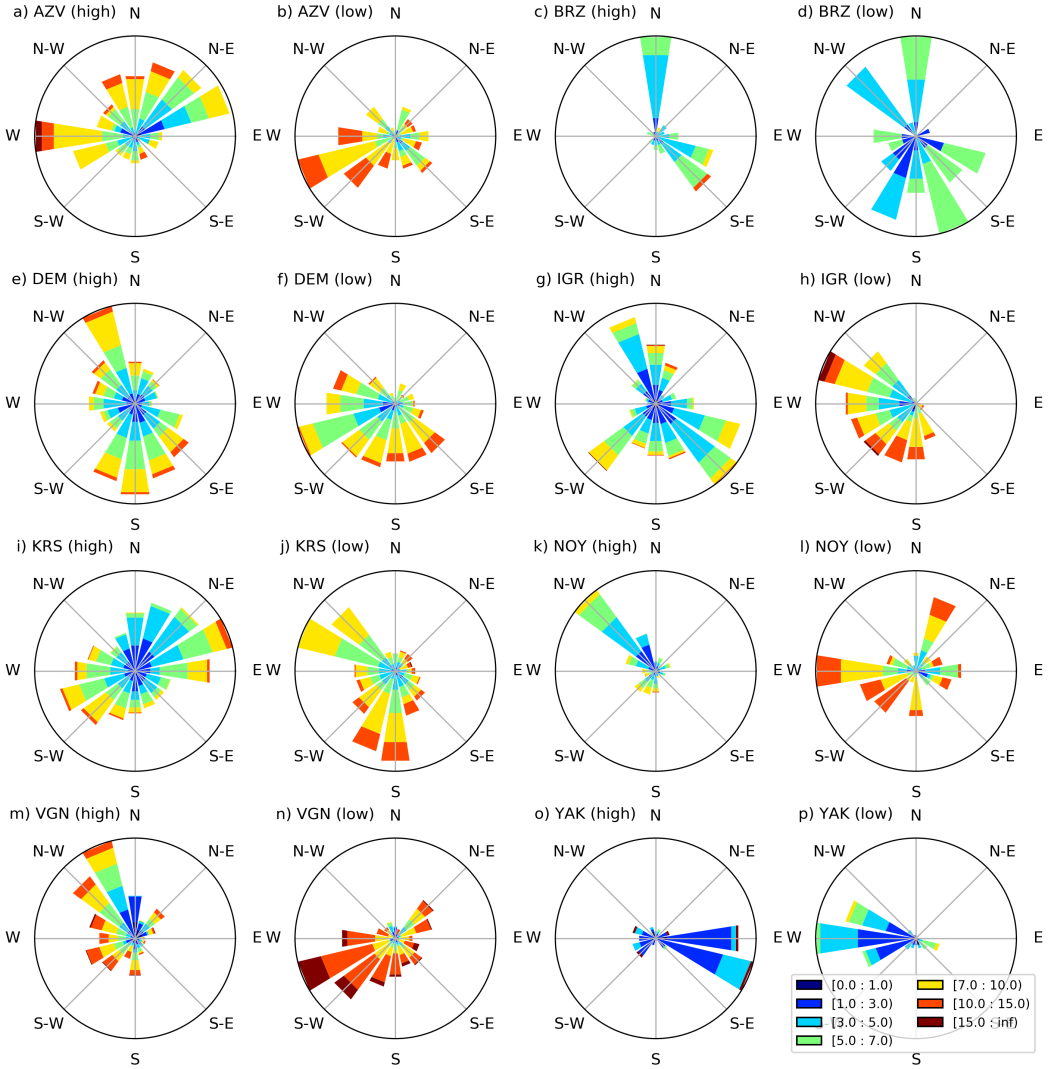

Figure 11. Wind roses depicting wind speed (m/s) and wind direction for high- and low-concentration CH_4 events for the considered measurement sites.

4. Conclusions

In this study, we present a time-series analysis of composite CO_2 and CH_4 concentration records from nine tower measurement sites in Siberia. The use of the Prophet model facilitates the analysis of a time-series of tracer concentrations and meteorological parameters. It helps to extract trends and periodic signals with different time scales and to filter out noise and outliers from datasets. Although it is challenging to quantify local sources and sinks of CO_2 and CH_4, we detected multi-year variability of tracers and identified events of elevated concentration. The periodicity of such events was found to vary throughout the year and to be different for CO_2 and CH_4, reaching up to 20% of days in some months. Furthermore, the weather conditions associated with elevated concentrations were analyzed. In most cases, elevated concentration events were caused by a temperature inversion and low wind speed. It was revealed that certain wind directions were correlated with high- and low-concentration events. For some sites, the wind direction was found to indicate the location of the sources of CO_2 and CH_4. To identify the type of source (natural or anthropogenic), additional information (e.g., CO mixing ratio) is needed. Currently, fairly simple criteria are used to filter observational data, such as excluding nighttime data and data obtained during low wind speeds and temperature inversions [9,11]. This analysis can be used to develop advanced criteria to filter observations used in inverse modeling.

Author Contributions: Conceptualization, methodology, formal analysis, and original draft preparation: D.B.; discussion, writing review and editing: M.A., B.B., D.D., A.F., M.S., and T.M.; preparation of measurement equipment, observation sampling and data primary processing: M.A., B.B., D.D., A.F., M.S. and T.M.

Funding: This research was supported by the Environment Research and Technology Development Fund (2-1802) of the Environmental Restoration and Conservation Agency of Japan. M.A., B.B., D.D., and A.F. are partly supported by the Ministry of Education and Science of the Russian Federation under State Contract No 14.613.21.0082 (ID No RFMEFI61317X0082).

Acknowledgments: The used data are available from the Global Environmental Database, hosted by Center for Global Environmental Research (CGER), National Institute for Environmental Studies (NIES) (http://db.cger.nies.go.jp/portal/geds/index). CarbonTracker CT2016 results provided by National Oceanic and Atmospheric Administration (NOAA) Earth System Research Laboratory (ESRL), Boulder, Colorado, USA from the website at http://carbontracker.noaa.gov.

Conflicts of Interest: The authors declare no conflict of interest.

Abbreviations

The following abbreviations are used in this manuscript:

CO_2 carbon dioxide
CH_4 methane

References

1. Kurganova, I.; Kudeyarov, V.; Gerenyu, L.D. Updated estimate of carbon balance on Russian territory. *Tellus Chem. Phys. Meteorol.* **2010**, *62*, 497–505. [CrossRef]
2. Le Quéré, C.; Andrew, R.M.; Friedlingstein, P.; Sitch, S.; Hauck, J.; Pongratz, J.; Pickers, P.A.; Korsbakken, J.I.; Peters, G.P.; Canadell, J.G.; et al. Global Carbon Budget 2018. *Earth Syst. Sci. Data* **2018**, *10*, 2141–2194. [CrossRef]
3. Sasakawa, M.; Shimoyama, K.; Machida, T.; Tsuda, N.; Suto, H.; Arshinov, M.; Davydov, D.; Fofonov, A.; Krasnov, O.; Saeki, T.; et al. Continuous measurements of methane from a tower network over Siberia. *Tellus Chem. Phys. Meteorol.* **2010**, *62*, 403–416. [CrossRef]
4. Lloyd, J.; Langenfelds, R.L.; Francey, R.J.; Gloor, M.; Tchebakova, N.M.; Zolotoukhine, D.; Brand, W.A.; Werner, R.A.; Jordan, A.; Allison, C.A.; et al. A trace-gas climatology above Zotino, central Siberia. *Tellus Chem. Phys. Meteorol.* **2002**, *54*, 749–767. [CrossRef]

5. Arshinov, M.Y.; Belan, B.; Davydov, D.; Inoue, G. Spatio-temporal variability of CO_2 and CH_4 concentration in the surface atmospheric layer over West Siberia. *Opt. Atmos. Okeana* **2009**, *22*, 183–192.
6. Arshinov, M.Y.; Belan, B.; Davydov, D.; Inouye, G.; Maksyutov, S.; Machida, T.; Fofonov, A. Vertical distribution of greenhouse gases above Western Siberia by the long-term measurement data. *Atmos. Ocean. Opt.* **2009**, *22*, 316–324. [CrossRef]
7. Sasakawa, M.; Machida, T.; Tsuda, N.; Arshinov, M.; Davydov, D.; Fofonov, A.; Krasnov, O. Aircraft and tower measurements of CO_2 concentration in the planetary boundary layer and the lower free troposphere over southern taiga in West Siberia: Long-term records from 2002 to 2011. *J. Geophys. Res. Atmos.* **2013**, *118*, 9489–9498. [CrossRef]
8. Sasakawa, M.; Machida, T.; Ishijima, K.; Arshinov, M.; Patra, P.; Ito, A.; Aoki, S.; Petrov, V. Temporal Characteristics of CH_4 Vertical Profiles Observed in the West Siberian Lowland Over Surgut From 1993 to 2015 and Novosibirsk From 1997 to 2015. *J. Geophys. Res. Atmos.* **2017**, *122*, 11–261. [CrossRef]
9. Saeki, T.; Maksyutov, S.; Sasakawa, M.; Machida, T.; Arshinov, M.; Tans, P.; Conway, T.; Saito, M.; Valsala, V.; Oda, T.; et al. Carbon flux estimation for Siberia by inverse modeling constrained by aircraft and tower CO_2 measurements. *J. Geophys. Res. Atmos.* **2013**, *118*, 1100–1122. [CrossRef]
10. Berchet, A.; Pison, I.; Chevallier, F.; Paris, J.D.; Bousquet, P.; Bonne, J.L.; Arshinov, M.Y.; Belan, B.; Cressot, C.; Davydov, D.; et al. Natural and anthropogenic methane fluxes in Eurasia: A mesoscale quantification by generalized atmospheric inversion. *Biogeosciences* **2015**, *12*, 5393–5414. [CrossRef]
11. Thompson, R.L.; Sasakawa, M.; Machida, T.; Aalto, T.; Worthy, D.; Lavric, J.V.; Lund Myhre, C.; Stohl, A. Methane fluxes in the high northern latitudes for 2005–2013 estimated using a Bayesian atmospheric inversion. *Atmos. Chem. Phys.* **2017**, *17*, 3553–3572. [CrossRef]
12. Taylor, S.J.; Letham, B. Forecasting at scale. *Am. Stat.* **2018**, *72*, 37–45. [CrossRef]
13. Papacharalampous, G.; Tyralis, H.; Koutsoyiannis, D. Predictability of monthly temperature and precipitation using automatic time series forecasting methods. *Acta Geophys.* **2018**, *66*, 807–831. [CrossRef]
14. Zhao, N.; Liu, Y.; Vanos, J.K.; Cao, G. Day-of-week and seasonal patterns of PM2.5 concentrations over the United States: Time-series analyses using the Prophet procedure. *Atmos. Environ.* **2018**, *192*, 116–127. [CrossRef]
15. Carbontracker-ch4. Available online: http://www.esrl.noaa.gov/gmd/ccgg/carbontracker-ch4/ (accessed on 1 November 2019).
16. Peters, W.; Jacobson, A.R.; Sweeney, C.; Andrews, A.E.; Conway, T.J.; Masarie, K.; Miller, J.B.; Bruhwiler, L.M.; Pétron, G.; Hirsch, A.I.; et al. An atmospheric perspective on North American carbon dioxide exchange: CarbonTracker. *Proc. Natl. Acad. Sci. USA* **2007**, *104*, 18925–18930. [CrossRef]
17. Watai, T.; Machida, T.; Shimoyama, K.; Krasnov, O.; Yamamoto, M.; Inoue, G. Development of an atmospheric carbon dioxide standard gas saving system and its application to a measurement at a site in the West Siberian forest. *J. Atmos. Ocean. Technol.* **2010**, *27*, 843–855. [CrossRef]
18. Suto, H.; Inoue, G. A new portable instrument for in situ measurement of atmospheric methane mole fraction by applying an improved tin dioxide–based gas sensor. *J. Atmos. Ocean. Technol.* **2010**, *27*, 1175–1184. [CrossRef]
19. Friborg, T.; Soegaard, H.; Christensen, T.R.; Lloyd, C.R.; Panikov, N.S. Siberian wetlands: Where a sink is a source. *Geophys. Res. Lett.* **2003**, *30*, 2129–2133. [CrossRef]
20. Panikov, N.S.; Dedysh, S. Cold season CH_4 and CO_2 emission from boreal peat bogs (West Siberia): Winter fluxes and thaw activation dynamics. *Glob. Biogeochem. Cycles* **2000**, *14*, 1071–1080. [CrossRef]
21. Bohn, T.J.; Melton, J.R.; Ito, A.; Kleinen, T.; Spahni, R.; Stocker, B.; Zhang, B.; Zhu, X.; Schroeder, R.; Glagolev, M.V.; et al. WETCHIMP-WSL: Intercomparison of wetland methane emissions models over West Siberia. *Biogeosciences* **2015**, *12*, 3321–3349. [CrossRef]
22. Repo, E.; Huttunen, J.T.; Naumov, A.V.; Chichulin, A.V.; Lapshina, E.D.; Bleuten, W.; Martikainen, P.J. Release of CO_2 and CH_4 from small wetland lakes in western Siberia. *Tellus Chem. Phys. Meteorol.* **2007**, *59*, 788–796. [CrossRef]
23. Harvey, A.C.; Peters, S. Estimation procedures for structural time series models. *J. Forecast.* **1990**, *9*, 89–108. [CrossRef]

24. Harvey, A.C.; Shephard, N. 10 Structural time series models. In *Econometrics*; Handbook of Statistics; Elsevier: Amsterdam, The Netherlands, 1993; Volume 11, pp. 261–302. [CrossRef]
25. The Prophet Package. Available online: https://facebook.github.io/prophet/ (accessed on 1 November 2019).
26. Annual Mean Growth Rate for Mauna Loa, Hawaii. Available online: https://www.esrl.noaa.gov/gmd/ccgg/trends/gr.html (accessed on 1 November 2019).
27. Dlugokencky, E.; Bruhwiler, L.; White, J.; Emmons, L.; Novelli, P.C.; Montzka, S.A.; Masarie, K.A.; Lang, P.M.; Crotwell, A.; Miller, J.B.; et al. Observational constraints on recent increases in the atmospheric CH_4 burden. *Geophys. Res. Lett.* **2009**, *36*. [CrossRef]
28. Nisbet, E.; Dlugokencky, E.; Manning, M.; Lowry, D.; Fisher, R.; France, J.; Michel, S.; Miller, J.; White, J.; Vaughn, B.; et al. Rising atmospheric methane: 2007–2014 growth and isotopic shift. *Glob. Biogeochem. Cycles* **2016**, *30*, 1356–1370. [CrossRef]
29. Arshinov, M.; Afonin, S.; Belan, B.; Belov, V.; Gridnev, Y.; Davydov, D.; Nedelec, P.; Paris, J.D.; Fofonov, A. Comparison between satellite spectrometric and aircraft measurements of the gaseous composition of the troposphere over Siberia during the forest fires of 2012. *Izv. Atmos. Ocean. Phys.* **2015**, *50*, 916–928. [CrossRef]
30. Umezawa, T.; Machida, T.; Aoki, S.; Nakazawa, T. Contributions of natural and anthropogenic sources to atmospheric methane variations over western Siberia estimated from its carbon and hydrogen isotopes. *Glob. Biogeochem. Cycles* **2012**, *26*. [CrossRef]
31. Worthy, D.; Levin, I.; Trivett, N.; Kuhlmann, A.; Hopper, J.; Ernst, M. Seven years of continuous methane observations at a remote boreal site in Ontario, Canada. *J. Geophys. Res. Atmos.* **1998**, *103*, 15995–16007. [CrossRef]
32. Public Holidays in Russia. Available online: https://en.wikipedia.org/wiki/Public_holidays_in_Russia (accessed on 1 November 2019).
33. Oberlander, E.A.; Brenninkmeijer, C.; Crutzen, P.; Elansky, N.; Golitsyn, G.; Granberg, I.; Scharffe, D.; Hofmann, R.; Belikov, I.; Paretzke, H.; et al. Trace gas measurements along the Trans-Siberian railroad: The TROICA 5 expedition. *J. Geophys. Res. Atmos.* **2002**, *107*. [CrossRef]
34. Hollinger, D.; Kelliher, F.; Schulze, E.D.; Bauer, G.; Arneth, A.; Byers, J.; Hunt, J.; McSeveny, T.; Kobak, K.; Milukova, I.; et al. Forest–atmosphere carbon dioxide exchange in eastern Siberia. *Agric. For. Meteorol.* **1998**, *90*, 291–306. [CrossRef]
35. Tashman, L.J. Out-of-sample tests of forecasting accuracy: An analysis and review. *Int. J. Forecast.* **2000**, *16*, 437–450. [CrossRef]
36. Turnbull, J.; Miller, J.; Lehman, S.; Tans, P.; Sparks, R.; Southon, J. Comparison of $14CO_2$, CO, and SF_6 as tracers for recently added fossil fuel CO_2 in the atmosphere and implications for biological CO_2 exchange. *Geophys. Res. Lett.* **2006**, *33*, L01817. [CrossRef]
37. Zhang, F.; Zhou, L.; Conway, T.J.; Tans, P.P.; Wang, Y. Short-term variations of atmospheric CO_2 and dominant causes in summer and winter: Analysis of 14-year continuous observational data at Waliguan, China. *Atmos. Environ.* **2013**, *77*, 140–148. [CrossRef]
38. Basu, S.; Baker, D.F.; Chevallier, F.; Patra, P.K.; Liu, J.; Miller, J.B. The impact of transport model differences on CO_2 surface flux estimates from OCO-2 retrievals of column average CO_2. *Atmos. Chem. Phys.* **2018**, *18*, 7189–7215. [CrossRef]
39. Baklanov, A.A.; Penenko, V.V.; Mahura, A.G.; Vinogradova, A.A.; Elansky, N.F.; Tsvetova, E.A.; Rigina, O.Y.; Maksimenkov, L.O.; Nuterman, R.B.; Pogarskii, F.A.; et al. Aspects of atmospheric pollution in Siberia. In *Regional Environmental Changes in Siberia and Their Global Consequences*; Springer: Berlin/Heidelberg, Germany, 2013; pp. 303–346.